Journal of the European Ceramic Society 20 (2000) 1069–1076

Pressureless sintering of fluorapatite under oxygen atmosphere

F. Ben Ayed[a,*], J. Bouaziz[a], K. Bouzouita[b]

[a]*Laboratiore de Chimie Industrielle, Equipe Matériaux Céramiques, Ecole Nationale d'Ingénieurs de Sfax, BP W 3038 Sfax, Tunisia*
[b]*Institut Préparatoire aux Etudes d'Ingénieur de Monastir, Route de Skanés 5000, Monastir, Tunisia*

Received 3 March 1999; received in revised form 29 September 1999; accepted 6 October 1999

Abstract

Fluorapatite (Fap) is prepared by precipitation method and sintering in the temperature range 640–1365°C. Linear shrinkage starts at about 715°C and the material reaches its final density at 890°C. Above this value, grain growth becomes important and induces an intragranular porosity which is responsible for density decrease. At 1180°C, a liquid phase is formed as a result of the formation of a binary eutectic between Fap and fluorite contained in the powder as impurity. This liquid phase further promotes the coarsening process and induces formation of large pores at high temperatures.

Keywords: Apatite; Fluorapatite; Grain growth; Microstructure-final; Porosity; Sintering

1. Introduction

Because of its chemical composition and crystallographic structure similar to those of hard tissues in vertebrate animals and humans, hydroxyapatite has been extensively studied for use as bone implants. Most studies are devoted to the knowledge of the sintering behaviour.[1–16] On the contrary little work has been reported on fluorapatite (Fap) densification[17–21] which also constitutes a potential candidate for several biological applications. Indeed, Fap presents interesting properties such as biocompatibility, solubility smaller than Hap's, or aptitude to delay caries' processes.[22,23] The aim of the present work is to study the sintering of pure fluorapatite under oxygen atmosphere.

2. Experimental procedure

2.1. Preparation and characterization of fluorapatite powder

The starting material is prepared by precipitation method.[24] A calcium nitrate solution is slowly added to a boiling solution containing diammonium phosphate and ammonium fluoride, with continuous magnetic stirring. During the reaction, pH is adjusted to the same level (pH 8–9) by adding ammonia. The obtained precipitate is filtered and washed with deionised water; it is then dried at 70°C for 12 h. The resulting powder is calcined in nitrogen gas flow at 500, 700 and 900°C at the rate of 10°C cm^{-1}. The samples are held for 1 h at fixed temperatures.

The chemical composition is determined by chemical analysis methods.[25,26] Specific surface areas of calcined powder are measured by the BET method using N_2 as an adsorption gas (ASAP200). The crystalline phases are identified by powder X-ray diffraction (XRD) using Cu K_α radiation (Seifert XRD 3000TT), and are checked with reference to the JCPDS cards. The powder is also submitted to infrared spectrometric (IR) analysis (Perkin–Elmer 783). To detect calcia, the phenolphthalein test (Afnor S94-066) is used. Differential thermal analysis, and thermogravimetry are carried out using about 30 mg of powder in oxygen (DTA–TG; Model Setaram). The heating rate is 5°C min^{-1}.

2.2. Preparation and characterization of ceramic specimens

The sintered powder, calcined at 500°C, is uniaxially pressed at 200 MPa to form pellets 13 mm in diameter and 1.5 mm thick. Green density reached about 60% of

* Corresponding author.

0955-2219/00/$ - see front matter
PII: S0955-2219(99)00272-1

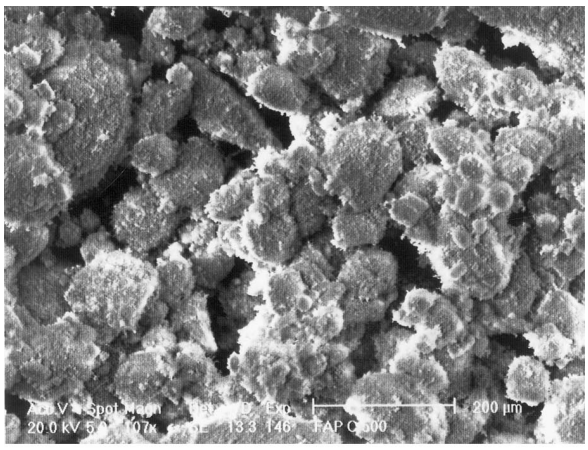

(a)

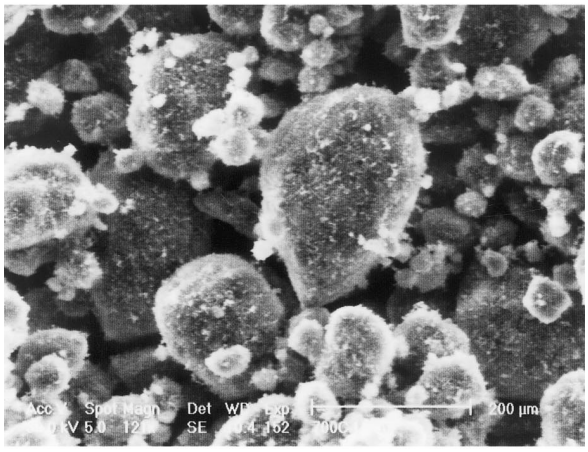

(b)

Fig. 1. S.E.M. micrographs of samples calcined for 1 h at: (a) 500°C; (b) 700°C.

the theoretical density, which is assumed to be 3.19. Linear shrinkage is determined by dilatometry (Setaram TMA 92 dilatometer) using the same thermal cycle as the one used for ATD and TG. The green compacts are pressureless sintered in a super Khantal furnace with oxygen flow at different temperatures. The heating rate is 10°C min^{-1}. The heating time is measured from the point at which the furnace reaches the heating temperature.

Bulk density of the sintered body is calculated from the dimensions and weight. The obtained products are examined with a scanning electron microscope (PHILIPS XL30) and analysed by X-ray powder diffraction.

Table 1
Calcination temperature dependence of grain size

	Diameter of powder calcined at 500°C (µm)	Diameter of powder calcined at 700°C (µm)
Agglomerates	140	180
Fine particles	20	40

Table 2
Evolution of the specific surface area and average grain size of Fap powders as a function of calcination temperature

Temperature (°C)	Specific surface area (m^2/g)	Average grain size (µm)
500	29	0.065
700	16.6	0.113
900	3	0.627

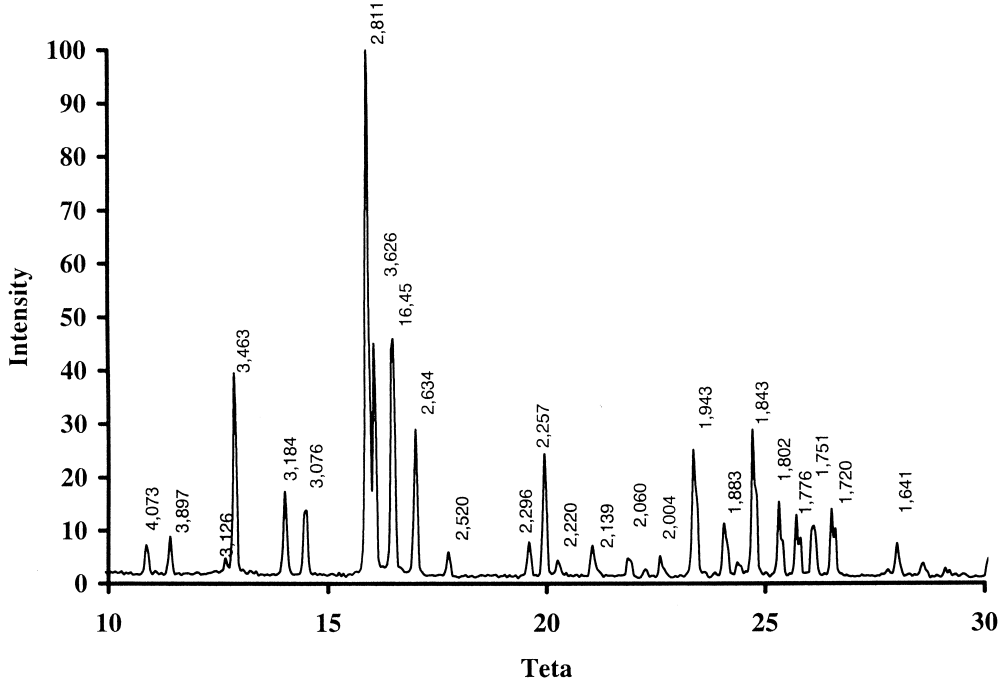

Fig. 2. XRD pattern of fluorapatite powder calcined at 900°C.

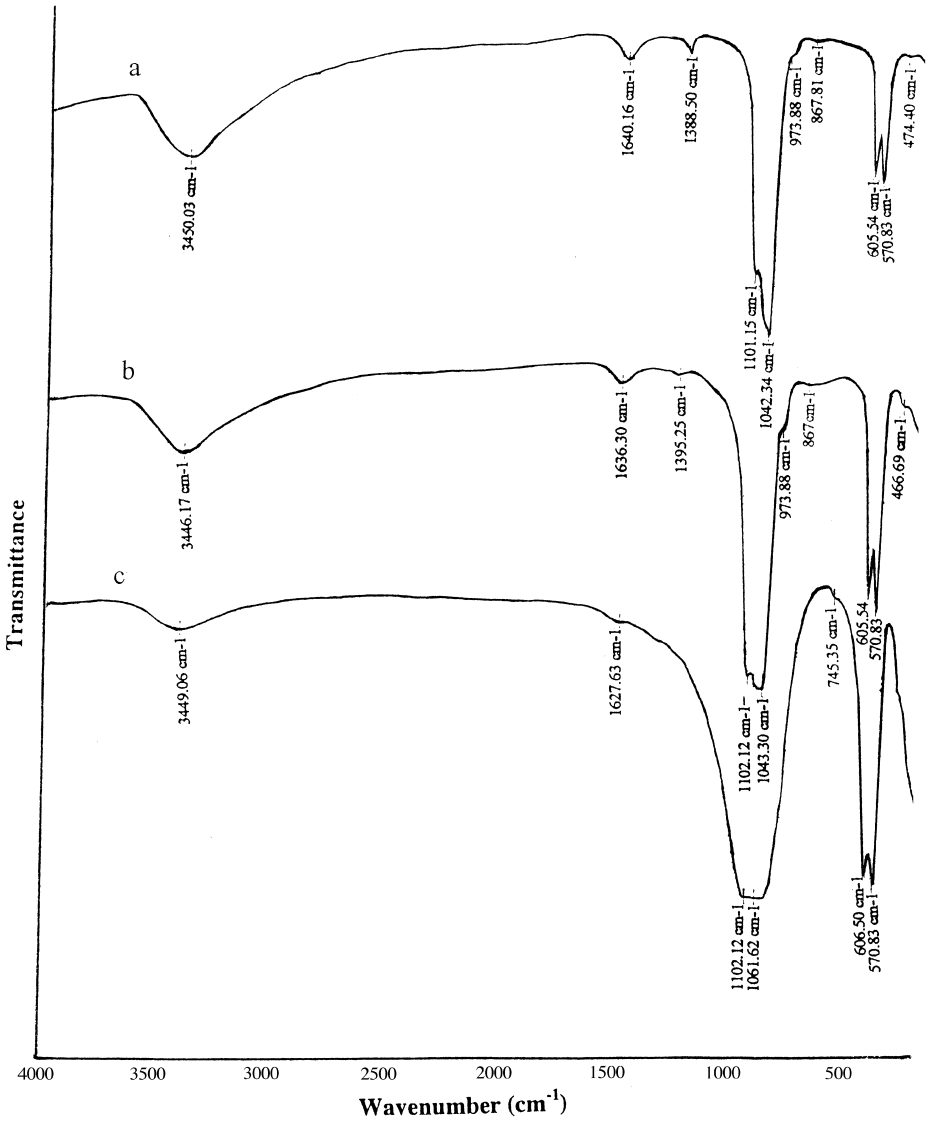

Fig. 3. IR spectra of fluorapatite powder: (a) unfired; (b) calcined at 500°C; (c) calcined at 900°C.

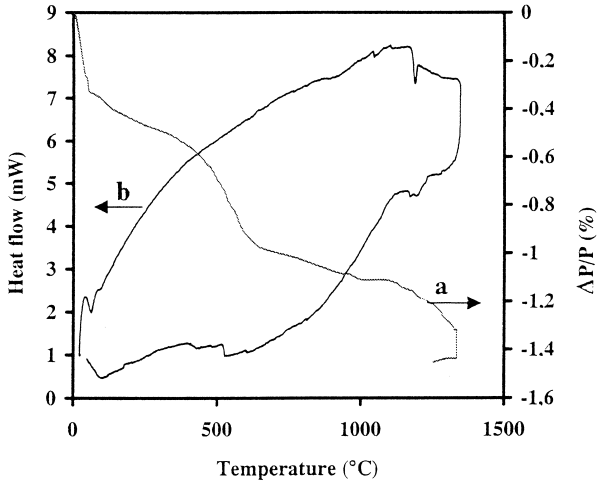

Fig. 4. TGA and DTA curves of fluorapatite powder calcined at 500°C.

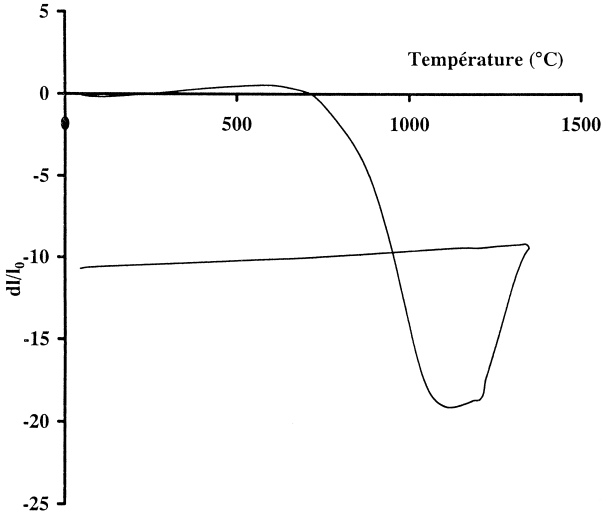

Fig. 5. Linear shrinkage versus temperature of fluorapatite precalcined at 500°C.

3. Results and discussion

3.1. Characterization of Fap powder

To improve crystallization state, powder is calcined under a nitrogen atmosphere at different temperatures such as 500, 700 and 900°C for 1 h. The obtained powders are observed by S.E.M. Typical micrographs are shown in Fig. 1. The powder obtained is composed of both agglomerates and fine particles with their diameters given in Table 1. Specific surface area is estimated for the powders; assuming the prepared calcined powder particles to be spherical in shape, the average sizes are calculated. From Table 2 the surface area of the calcined powders is found to decrease as calcination temperature increases, due to particle size increases. Bernache et al.[21] demonstrated that the grain growth occurs through a mechanism of superficial diffusion. Note that these specific surface area values do not correspond to particle size observed by S.E.M. (Fig. 1); this discrepancy may be due to the presence of micropores formed by of residual species' release.

The Ca/P ratio determined by chemical analysis is 1.66. XRD diagram reported in Fig. 2 reveals only peaks of Fap. However, it is not possible to exclude the presence of impurities in the powder. Indeed, it is well known that XRD analysis does not enalk to disclose in apatites impurity less than 2%.[27] On the other hand, as

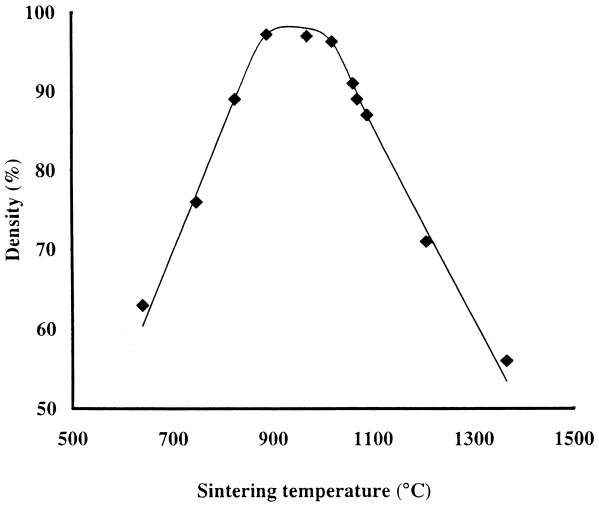

Fig. 6. Relative density versus temperature of samples sintered for 1 h.

Table 3
Relative density versus temperature of sintered samples

Sintering temperature (°C)	Density (%)
640	63
760	76
825	89
890	97.2
970	97
1020	96.3
1050	91
1070	89
1090	87
1170	71
1365	56

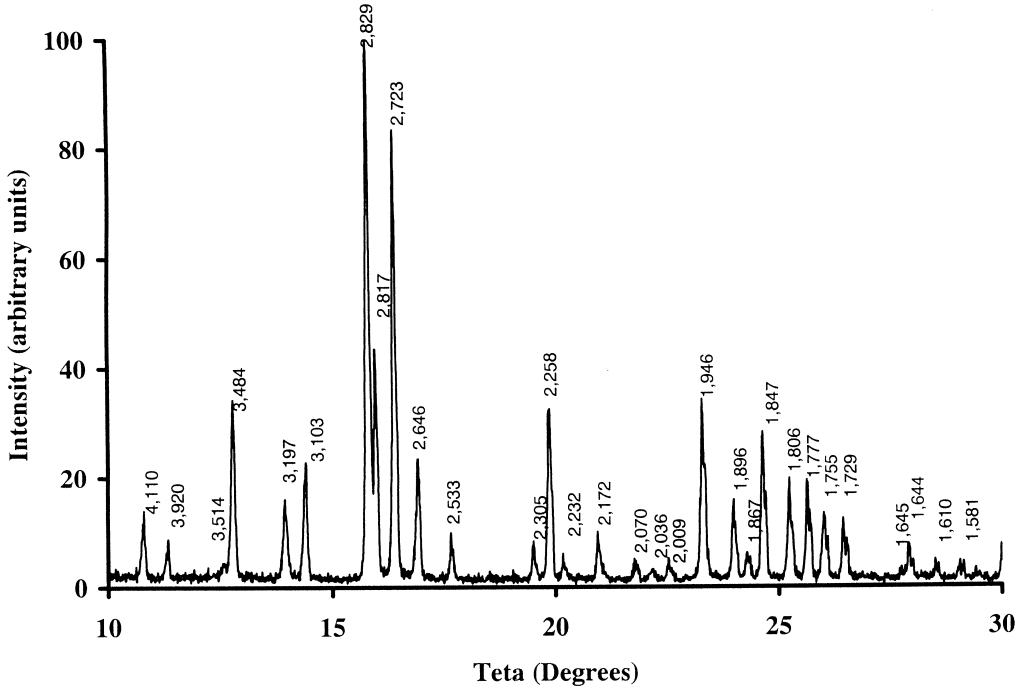

Fig. 7. XRD pattern of sample sintered at 1365°C for 1 h.

indicated by Heughebart,[28] it is difficult to prepare the composition corresponding to Ca/P = 1.67 ratio. So formation of secondary phases such as calcia (CaO) or fluorite (CaF_2) would occurr during powder preparation. The negative test of phenolphtalein suggests that calcia is not present in the powder, whereas the presence of fluorite remains, probably, all the more as this compound is transparent to infrared radiations.

On the same powder, FTIR spectroscopic analysis is also performed. Typical results of dried and calcined powders are shown in Fig. 3. In all the spectra, the absorption peaks at 3450 and 1640 cm^{-1} are assigned to the adsorbed water, whereas those at 474, 570, 605 and 900–1100 cm^{-1} to PO_4^{-3} group. The additional absorptions detected at 867 and 1388 cm^{-1}, in the case of unfired powder, are assigned, respectively, to HPO_4^{2-} and NO_3^- (Fig. 3(a) and (b)). The absorption at 745 cm^{-1} detected on the spectra of powder calcined at 900°C (Fig. 3(c)), is assigned to $P_2O_7^{4-}$ group which results from the decomposition of HPO_4^{2-} according to the reaction: $2HPO_4^{2-} \rightarrow P_2O_7^{4-} + H_2O$.

TGA and DTA studies are carried out to analyse weight loss and detect a potential phase change during the sintering of powder calcined at 500°C. Typical TG and DTA curves are given in Fig. 4. It can be observed that there are two weight losses [Fig. 4(a)]. The first weight loss, below 250°C, corresponds to the removal of water and the next one, between 250 and 650°C, is due to the decomposition of the NO_3^- and HPO_4^{2-} species. The final weight loss is about 1.3%. The DTA curve [Fig. 4(b)] contains two endothermic peaks. The peak around 110°C is due to the departure of adsorbed water as observed in the TGA curve. The decomposition of nitrate has not been resolved in the DTA curve, but it has been confirmed by IR spectra which indicates that the absorption peaks assigned to NO_3^- and HPO_4^{2-} disappear when temperature exceeds 500°C [Fig. 3(c)]. The second peak around 1180°C may be due to the formation of a liquid phase on account of the sample's vitreous appearance after cooling. Note that fluorapatite has a very high thermodynamic melting point (1640°C). Under these conditions, the liquid phase could be probably formed from binary eutectic between

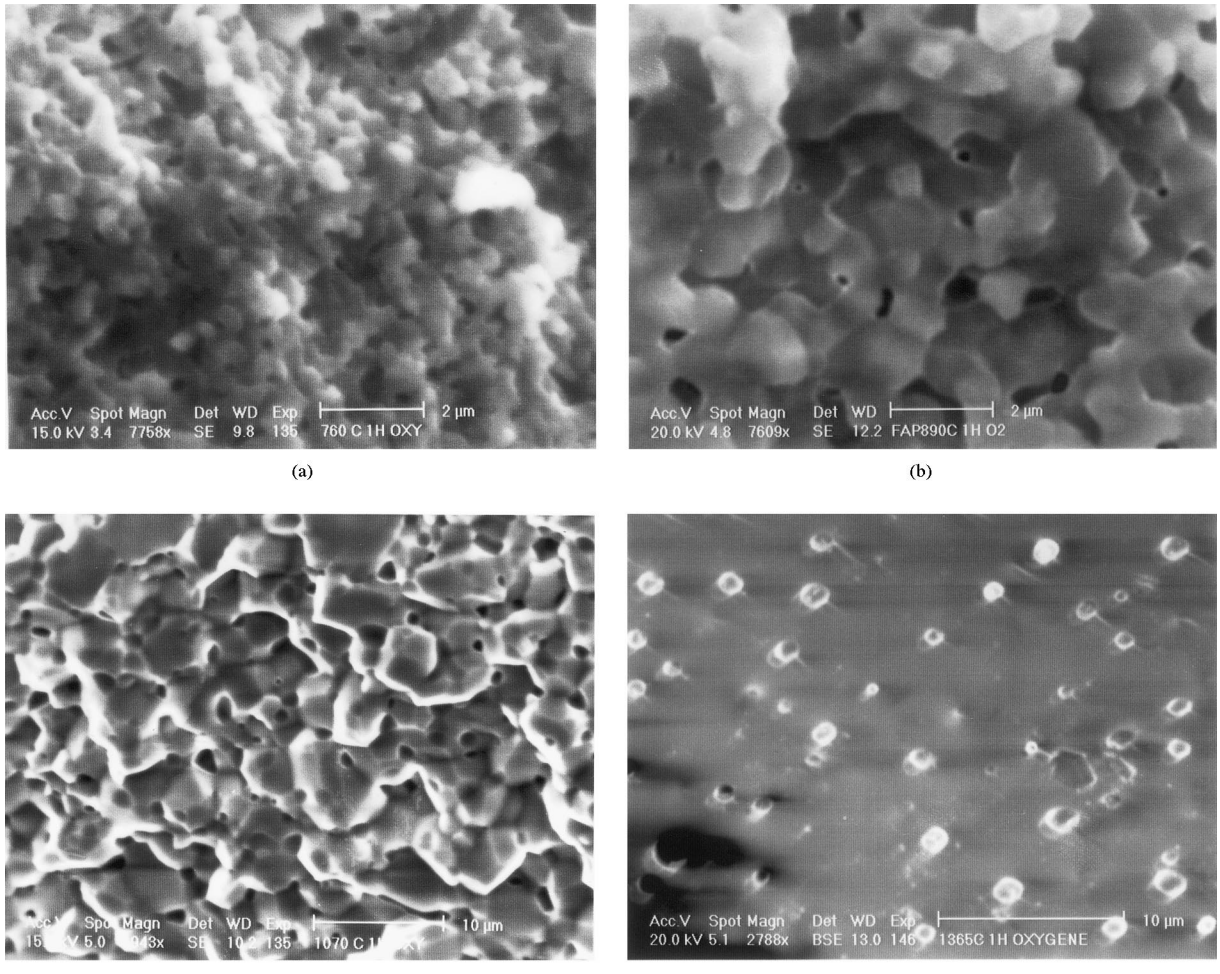

Fig. 8. S.E.M. micrographs of samples sintered for 1 h at: (a) 640°C; (b) 890°C; (c) 1070°C; (d) 1365°C.

Fap and impurities contained in the powder. The binary phase diagram of fluorite and tricalcium phosphate[23] indicates the formation of an eutectic between CaF_2 and $Ca_{10}(PO_4)_6F_2$ at 1210 ± 5°C. In the present case, eutectic can take place if fluorite is assumed to be formed as a second phase during the powder preparation.

3.2. Sintering of Fap

In order to examine the powder's densification behaviour during the heating process, the linear shrinkage of a compact is measured. Fig. 5 shows that shrinkage starts at about 715°C and continues up to 1090°C. The total shrinkage in this range of temperature achieves 19%. Above 1200°C, a large expansion (8%) takes place, which is probably the following of the liquid phase formation and the evaporation of volatiles produced by Fap decomposition.

The effect of temperature is studied between 640 and 1365°C for 1 h. Fig. 6 shows that relative density increases rapidly from 640 to 890°C; it then remains practically constant up to 1020°C; and finally decreases above this value. As shown in Table 3, relative density reaches 97.2% of the theoretical density at 890°C, and it is only about 56% at 1365°C. It is lower than the green density.

Regardless of temperature, XRD analysis of the obtained products reveals the presence of Fap without any other structures (Fig. 7). As expected, we note an increase in Fap crystallinity as temperature rises.

Fig. 8 shows S.E.M. micrographs of the fracture surfaces of samples sintered at 640, 890, 1070 and 1365°C. The fracture surfaces clearly reveal a distinct difference in the samples' microstructure. Fig. 8(a), shows that at 640°C, the sample presents an important intergranular porosity subsequently eliminated, with the grain growth (Fig. 8(b)). In this temperature range, the grains have a polyhedral form with a diameter of 0.4 μm at 640°C and 1 μm at 890°C. Thus, a slight coarsening accompanies densification. When temperature increases, the grains' growth becomes exaggerated, the average grains' size is about 5 μm at 1070°C [Fig. 8(c)]. Note that the microstructure exhibits many intragranular pores which tend to evolve into spherical shapes. Such a porosity, which is responsible for the decrease in density above 1020°C, is also observed by both A Binder-Royer[7] and Ababou[13] during the sintering of Hap. In their studies, complete densification could not be also reached.

No densification occurs in parallel with the liquid phase formation. In general, the liquid phase is used to promote densification. But here, besides the coarsening during the increase in temperature up to the value at which liquid phase is formed, a presintering occurs, leading to a continuous skeleton which prevents rearrangement of Fap particles. As a result of the liquid phase formation, the coarsening becomes more important; it is facilitated by dissolution–reprecipitation processes.

At higher temperatures, besides the coarsening, densification is hindered by the formation of the large pores (Fig. 8d). During the study of the hot pressing reaction of fluorapatite, Franz et al.[20] also observed the formation of large pores at these temperatures. They attributed to the evaporation of volatiles produced by Fap decomposition. But in our study, the very small weight loss measured at those temperatures by TGA suggests that the pores are essentially due to the migration of the liquid out of the samples as result of the decrease in the liquid's viscosity. However, the decomposition of Fap and the volatilization of the result species is not excluded and may contribute to the pores formation. The spectra IR for samples sintered at

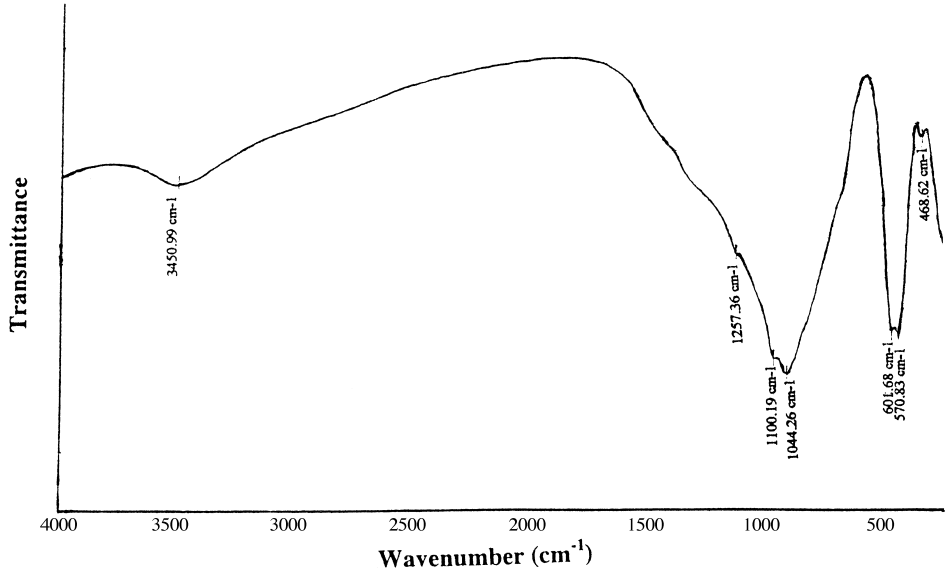

Fig. 9. IR spectra of fluorapatite sintered for 1 h at 1365°C.

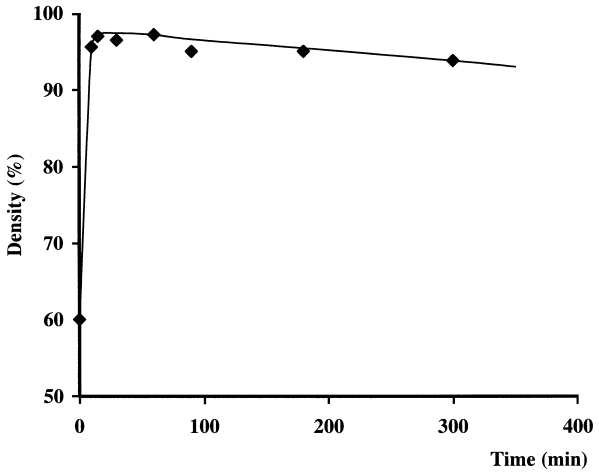

Fig. 10. Relative density versus sintering time at 890°C.

Table 4
Relative density versus time of samples sintered at 890°C

Time (min)	Density (%)
0	60
10	95.6
15	97
30	96.5
60	97.2
90	95
180	95
300	93.8

1365°C is slightly different from the spectra of powder calcined at 900°C. The little difference, can be explained by a waste of stoechiometic of the Fap (Fig. 9).

Time dependence of densification is shown in Fig. 10. Relative density reaches 95.6% after only 10 min of heat treatment, 97% after 15 min and remains practically constant for extended time. Nevertheless, a slight decrease in density is noted for longer time (Table 4). XRD of samples does not show any evolution in the nature of the crystalline phase with time. Microstructure examination of samples sintered for several times indicates, only a slight occurrence grain growth, not sufficient to lead to complete material densification, after longer exposure to temperature.

4. Conclusion

Fap presents good sinterability, since the material's ultimate density is attained after 15 min at 890°C. Samples' microstructure evolution is largely dominated by the coarsening of the Fap grains. At moderate temperatures ≈890°C, the material presents a homogeneous microstructure composed of polyhedral grains with small facets which would lead, normally, to good mechanical properties. When sintering time is increased, a slight grain coarsening occurs. However, no densification occurs in parallel with this coarsening. Also, increasing temperature does not enhance densification, on account probably of the coarsening which becomes important and induces an important intragranular porosity. At 1180°C, a liquid phase which accelerates the grain's growth is formed further to the formation of a binary eutectic between Fap and impurities contained in the powder such as CaF_2. Above 1200°C, pore formation is induced by the migration of the liquid phase out of the sample and the evaporation of volatiles due to the Fap decomposition.

Acknowledgements

The authors would like to thank I. Khattech for his assistance in preparing fluorapatite powder.

References

1. Jarcho, M., Belen, C. H., Thomas, M. B., Bobick, J., Kay, J. F. and Dormus, R. H., Hydroxyapatite synthesis and characterisation in dense polycrystalline from. *J. Mat. Sci*., 1976, **11**, 2027–2035.
2. Montel, G., Constitution et structure des apatites biologiques: influence de ces facteurs sur leurs propriétés. *Revue de biologie cellulaire*, 1977, **28**, 179–186.
3. Peelen, J. G. J., Redja, B. V. and Degroot, K., Preparation and properties of sintered hydroxyapatite. *Ceram. Int*., 1978, **4–2**, 71–74.
4. De With, G., Vandijk, H. H. A., Hattu, N. and Prijs, K., Preparation, microstructure and mechanical properties of dense polycrystalline hydroxyapatite. *J. Mat. Sci*., 1981, **16**, 1592–1598.
5. Asada, A. and Oukami, K., Affect of powder characterisation on the sinterability of calcium hydroxyapatite. *Yogyo- Kyokai- Shi*, 1987, **95–7**, 41–47.
6. Tamari, Nobuyuki, Kondo, Isao and Kinoshita, Makoto, Addition of effects of fluorides on sintering hydroxyapatite. *Funtai oyobi Funmaatsuyakin*, 1987, **34**(2), 91–94.
7. Binder-Royer, A., Etude de l'influence de la composition de l'hydroxyapatite frittée sur ses propriétés mécaniques. Thése de Doctorat, INPG, Grenoble, 1988.
8. Lin, F. H., Tzung-Li, H. and Hon, M. H., A study on synthesised hydroxyapatite bioceramic. *Ceram. Int*., 1989, **15**, 351–356.
9. Goto, T., Wakamatsu, N., Kamemizu, H., Doi, Y. and Moriwaki, Y., Sintering mechanism of hydroxyapatite by addition of lithium phosphate. *J. Mater. Sci*., 1991, **2**, 149–152.
10. Lelièvre, F., Etude du coulage et du frittage de l'hydroxyapatite, application à la réalisation de piéces cellulaires. Thése de Doctorat, Faculté des Sciences, Limoges, 1992.
11. Rabu, B., Contribution à l'étude de l'hydroxyapatite frittée: préparation et propriétés mécaniques du composite particulaire $Ca_5(PO_4)_3OH$–Ca_2SiO_4, Création de micropores par frittage sous pression. Thèse de Doctorat, INPG, 1992.
12. Pauchin, E., Wang, T. and Chaki, Sintering behaviour and mechanical properties of hydroxyapatite and dicalcium phosphate. *J. Mat. Sci. In Medicine*, 1993, **4**, 150–158.
13. Ababou, A., Etude expérimentale et théorique du préfrittage et du frittage de l'hydroxyapatite. Thèse de Doctorat, Faculté des Sciences, Limoges, 1994.

14. Santos, J. D., Silva, P. L., Knowles, J. C., Talal, S. and Monterio, F. J., Reinforcement of hydroxyapatite by adding P_2O_5–CaO glasses with Na_2O, K_2O and MgO. *J. Mat. Sci. In Medicine*, 1996, **8**, 187–189.
15. Cüneyttas, A., Korkusuz, F., Timuçin, M. and Akkas, N., An investigation of the chemical synthesis and high-temperature sintering behaviour of calcium hydroxyapatite and tricalcium phosphate bioceramics. *J. Mat. Sci. In Medicine*, 1997, **8**, 91–96.
16. Fanovich, M. A. and Porto Lôpez, J. M., Influence of temperature and additives on the microstructure and sintering behaviour of hydroxyapatite with different Ca/P ratios. *J. Mat. Sci. In Medicine*, 1998, **9**, 53–60.
17. Levitt, S. R., Crayton, P. H., Monroe, E. A. and ondrate, R. D., *J. Bromed. Mater. Res.*, 1969, **3**, 683–689.
18. Rajarao, W. and Boehem, R. F., A study on sintered apatites. *J. Dent.*, 1974, **53**(6), 1351–1355.
19. Duff, E. J. and Grant, A. A., Apatite ceramics for use in implantation. In *Adv. in Biomat., Vol. 2, Mechanical Properties of Biomaterials*. Wiley, 1980, pp. 465–475.
20. Franz, E. D. and Telle, R., Reaction hot pressing of fluorapatite for dental implants. *High Tech. Ceram.*, 1987, 31–41.
21. Sennamaud, N., Bernache-Assollant, D., Champion, E., Heughebaert, M. and Rey, C., Calcination and sintering of hydroxypatite powders. *Solid State Ionics*, 1997, **101–103**, 357–362.
22. Narasaraju, T. S. B., pH-dependence of solubility's of solid solutions of hydroxyapatite and fluorapatite. *Indian J. Chem.*, 1972, **10**, 308–309.
23. Franz, E. D., Fluorapatit $Ca_5F(PO_4)_3$ — Ein Modell Zur Synthese der Zahnhartsubstanz im system CaF_2 — $Ca_3(PO_4)_2$. *Z. Naturforschung*, 1983, **38b**, 1037–1040.
24. Henghebaert, J. C., Contribution à l'étude de l'évolution des orthophosphates de calcium précipités en orthophosphates apatitiques. Thèse, INP, Toulouse, 1977.
25. Charlot, G., *Les Méthodes de la Chimie Analytique, Analyse Quantitative et Minérale*. Masson, Paris, 1996.
26. Gee, A. and Deitz, V. R., Determination of phosphates by differential spectrometric. *Anal. Chem.*, 1953, **25**, 1320–1324.
27. Legeros, R. Z., Crystallography studies of the carbonate substitution in the apatite structure. Ph.D. thesis, New York, 1967.
28. Henghebaert, J. C., Biocéramiques constituées de Phosphate de Calcium. *Silicates Industriels*, 1988, **3–4**, 37–41.